Catalysis Today xxx (2016) xxx–xxx

Contents lists available at ScienceDirect

Catalysis Today

journal homepage: www.elsevier.com/locate/cattod

ATR-FTIR spectrokinetic analysis of the CO adsorption and oxidation at water/platinum interface

Alejo Aguirre, Claudio L.A. Berli, Sebastián E. Collins*

Instituto de Desarrollo Tecnológico para la Industria Química (INTEC), Universidad Nacional del Litoral, CONICET, Güemes 3450, S3000GLN Santa Fe, Argentina

ARTICLE INFO

Article history:
Received 18 September 2015
Received in revised form 9 March 2016
Accepted 11 March 2016
Available online xxx

Keywords:
Attenuated total reflection
Operando infrared spectroscopy
Mass transport
Catalyst layer
CO adsorption and oxidation on platinum

ABSTRACT

Attenuated total reflection infrared (ATR-IR) spectroscopy is a powerful tool to investigate reaction pathways in liquid(reactive)/solid(catalyst) systems. Catalysts are commonly deposited on an internal reflection elements (IRE) as layers of powders or as films (e.g. metal film), and they are exposed to the liquid phase reactants. To obtain quantitative information of intrinsic reaction rates, the chemical engineering aspects of an ATR flow-through cell must be evaluated. Particularly, mass transport in the ATR cell has to be characterized. We present here an analysis of the mass transfer from the flowing solution to the surface of the ATR crystal, where the catalyst is deposited. Criteria to determine kinetic parameters under chemical control were developed on the base of non-dimensional Péclet (*Pe*) and Sherwood (*Sh*) numbers, and Thiele modulus (φ_{cl}). A Pt thin film deposited on a ZnSe IRE by vapor deposition and a layer of Pt/Al_2O_3 porous catalyst were used to study the adsorption of carbon monoxide and oxidation of preadsorbed carbon monoxide on aqueous phase. Experimental data of the evolution of the linearly adsorbed CO (2048 cm^{-1}) were fitted using a microkinetic model to obtain reaction constants. Results reported here serve as a practical guide to quickly determine the operational limits of an ATR cell with a porous layer of catalyst deposited onto the IRE.

1. Introduction

Catalytic processes at liquid/solid interfaces are highly important in a number of chemical and biochemical systems. Spectroscopic studies using in situ or operando methods in the presence of the solvent are essential in order to postulate reliable reaction pathways with meaningful kinetic data [1]. This is because surface reactions in the presence of solvent do not necessarily proceed via the same mechanism, intermediates and/or energetic as compared with the gas phase reaction. Then, monitoring the catalytic reactions under realistic conditions and in a time-resolved mode is critical for understanding the reaction-structure relationships, and, as a consequence, for the rational design and optimization of new efficient catalytic systems.

In particular, water is the most import solvent. As recently highlighted in the compressive review of Shi et al. [2], monitoring surface processes at the water/catalyst interface is a challenging task. Even so, important advances have been achieved during the recent years, among which highlights vibrational, X-ray absorption and nuclear magnetic spectroscopies [3–10].

Infrared spectroscopy is an appropriate and important tool for the investigation of reaction pathways in liquid phase because it provides the selective detection of species adsorbed on a catalyst under reaction conditions [1,3,9,11]. Due to the fact that liquids are strong absorbers of infrared radiation, attenuated total reflection infrared (ATR-IR) spectroscopy is employed for studying molecular vibrations at the solid-liquid interface because the evanescent wave sense only the region near the interface, thereby minimizing the contribution from the liquid [1]. Usually, multiple internal reflection elements (IRE) with high geometrical surface area can be used in order to improve the signal-to-noise ratio. Thus, ATR can be used to track surface intermediate species and, moreover, it can be configured to feature a microreactor to measure reaction rates [12–14]. When an ATR cell -or any operando cell- is used for kinetic experiments it is necessary to ensure the absence of mass transfer limitation to obtain the intrinsic reaction rates or, simultaneously solve the kinetic and convention-diffusion model to fit the experimental data [15]. In an ATR cell, the catalyst is deposited onto the IRE crystal and the reactants have to be transported from the flowing bulk solution to the catalyst. This mass transfer has to be faster than the reaction; otherwise the reactant concentration at

* Corresponding author.
E-mail address: scollins@santafe-conicet.gov.ar (S.E. Collins).

http://dx.doi.org/10.1016/j.cattod.2016.03.042
0920-5861/

the catalyst surface is lower than that at the bulk and the reaction is limited by mass transport.

In a previous work we provided several design criteria for the construction of an optimized flow-through ATR cell for spectrokinetic analysis, and performed an analysis of the operative limits to obtain intrinsic kinetic information [16]. It was shown that the flow into the cell is characterized by a convection-diffusion transport model (laminar flow) and suitable criteria were established based on a dimensionless analysis in terms of Péclet (*Pe*), Biot (*Bi*) and Damköhler (*Da*) numbers [16].

In the case of a layer of porous catalyst deposited onto the ATR crystal, it is important to determine the external mass transport, i.e. the transport from the liquid phase to the film, but also, the internal mass transport, i.e. the diffusion into the porous layer, in order to obtain kinetic data under true chemical control. In this work we used the optimized flow-through ATR cell developed in our laboratory for transient experiments to study the adsorption and oxidation of CO on water/platinum interface in both non-porous and porous catalyst layers under chemical control. The operational limit of the ATR cell is characterized by means of a non-dimensional analysis in terms of Péclet number (*Pe*), Thiele modulus (φ_{cl}) and Sherwood number (*Sh*).

2. Materials and methods

2.1. Spectroscopic setup

ATR-FTIR spectra were recorded using a homebuilt stainless steel flow-through cell as described in detail elsewhere [16]. The optimized design of the ATR cell has linear-shaped entrance and exit ports close to the extremes of the cell to avoid dead-volume zones and to enable uniform fluid velocity profile across the cell, which is fully developed immediately after the ports. The total cell volume is 60 μL. The IRE is a 45° trapezoidal ZnSe crystal whose dimensions are 80 × 10 × 4 mm, providing 10 internal reflections at the liquid/crystal interface.

The cell was mounted onto an ATR attachment (Pike Technologies) inside the sample compartment of the FTIR spectrometer (Thermo-Electron, Nicolet 8700 with a cryogenic MCT detector). The bench of the spectrometer was continuously purged with dried air (Parker Balston FTIR purge gas generator) to eliminate CO_2 and water vapor contributions to the spectra. Time-resolved ATR-FTIR spectra were recorded in kinetic and rapid-scan mode at a resolution of 4 cm^{-1} (up to 1 spectrum/0.39 s). Liquids, provided from two separate bottles, were flowed through the cell using a pulse-free peristaltic pump (Ismatec ICP4) located at the end of the cell. A pneumatically actuated three-way valve controlled by a computer software allows to switch the stream of solutions. More details of the experimental setup can be found elsewhere [11]. Dissolved CO and O_2 in deionized water (18 MΩ) was provided from individual glass saturators, at controlled temperature, by bubbling CO (Aldrich 99.9999%) or O_2 (Matteson 99.999%) at 20 cm^3 min^{-1}. The concentration of dissolved gases in water was calculated based on reported solubility data at room temperature and gas pressure of 1 atm.

A non-porous platinum layer with a thickness of about 20 nm was prepared by vapor deposition on the ZnSe IRE. A film of Pt(0.38 wt.%)/γ-Al_2O_3 was prepared by dropping a suspension of 2 mg of the catalyst per mL of water. This suspension was previously dispersed during 4 h in ultrasonic bath.

In order to clear the platinum layer, the coated IRE was pretreated ex-situ under pure H_2 (50 cm^3/min) at 473 K for 2 h, and purged with He at the same temperature (30 min). Next the ZnSe crystal was fitted on the ATR cell and, after purging with He, was exposed again to H_2 (5%)/He at 293 K.

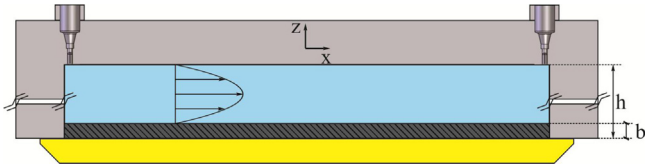

Fig. 1. Scheme of the flow-through ATR cell used in the present study. h stand for the height of the fluid compartment (h = 250 μm) and b stand for the height of the catalyst layer.

2.2. Mass transport modelling

The determination of intrinsic reaction rates in operando reactors requires the consideration chemical engineering aspects [15]. As stated in Section 1, optimized ATR cells allow one to measure kinetic process at liquid/solid interfaces, such as adsorption and surface reactions in heterogeneous catalysis. In this sense, the obtained data in transient experiments of this kind should be under chemical control, that is, ideally free of mass transport limitations. However, as it was analyzed in a previous work [16], a diffusion-convection regime governs the reactants transfer to the IRE surface where the catalyst is deposited. Therefore, the cell operational limits could be determined. Recently, a similar problem has been addressed by Gervais et al. [17] and by Hansen et al. [18] for the appropriate operation of surface-based sensors in microfluidic system based on surface plasmon resonance (SPR). However, for a catalytic process in a porous layer inside the ATR cell, the mass transport into the layer has to be considered. This problem is similar to the one present in microreactors [19–23], but with the particular geometry characteristics of the ATR cell.

The adsorption-desorption process in a porous film of deposited catalyst, considering both the bulk transport of reactants in the solution and the intra-particle diffusion, is analyzed as follows. The equation that describes the evolution of the surface concentration $\Gamma(x, z, t)$ is:

$$\frac{\partial \Gamma}{\partial t} = k_a C_i(\Gamma_0 - \Gamma) - k_d \Gamma \tag{1}$$

where k_a and k_d are the adsorption and desorption constants, respectively, C_i is the concentration of the solute in the bed, and Γ_0 is the total number of binding sites per surface area.

If mass transport limitations are present into the porous bed, the concentration C_i, and therefore the surface concentration Γ, will change in the *z*-direction as well. To quantify these transport limitations, the mass balance for the *i*-species has to be solved. Fig. 1 shows schematically the process into the ATR cell. It is worth to mention that we analyzed the relative importance of intra-particle gradients and concluded that this limitation is absent for the case analyzed here (see Supplementary information).

Considering a pseudo-homogenous model, the mass balance for *i*-species in the porous bed of height *b* is given by Froment et al. [24]:

$$0 < z < b;\ \frac{\partial C_i}{\partial t} = D_{eff}\left(\frac{\partial^2 C_i}{\partial z^2} + \frac{\partial^2 C_i}{\partial x^2}\right) - \varepsilon^{-1} a_v [k_a C_i(\Gamma_0 - \Gamma) - k_d \Gamma] \tag{2}$$

where D_{eff} is the effective diffusion coefficient in the porous bed, ε is the bed porosity, and a_v is the surface area of reaction per unit volume. It is worth to notice that the fluid into the catalyst film is stagnant in this model, that is, the fluid velocity is zero.

Initial and boundary conditions for Eq. (2) are:

$$x = 0;\ \frac{\partial C_i}{\partial x} = 0 \tag{3}$$

$$x = L;\ \frac{\partial C_i}{\partial x} = 0 \tag{4}$$

Please cite this article in press as: A. Aguirre, et al., ATR-FTIR spectrokinetic analysis of the CO adsorption and oxidation at water/platinum interface, Catal. Today (2016), http://dx.doi.org/10.1016/j.cattod.2016.03.042

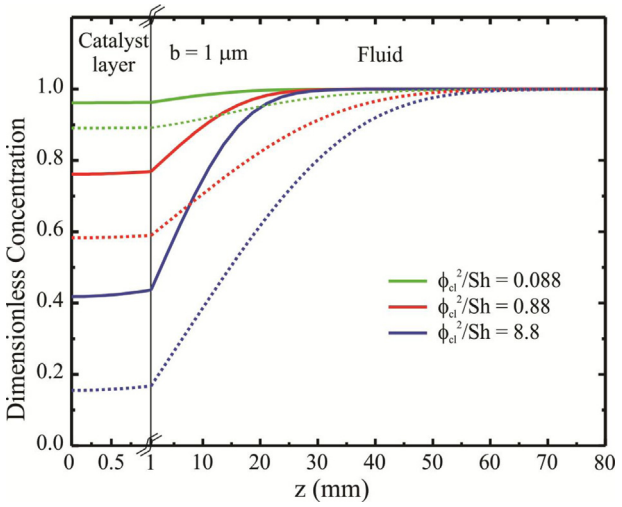

Fig. 2. Normalized concentration of a reactant (t = 12.5 s) as function of cell height, for different positions along the x-direction, near the entrance (1 cm, full lines) and near the exit (7 cm, dotted lines). Colors refer to ϕ_{cl}^2/Sh ratio: green 0.088; red 0.88; and blue 8.8. (For interpretation of the references to color in this figure legend, the reader is referred to the web version of this article.)

$$z = 0;\ \frac{\partial C_i}{\partial z} = 0 \tag{5}$$

$$t = 0;\ C_i = 0 \tag{6}$$

The mass balance for i-species in the cell of height h is given by Froment et al. [24] and Bird et al. [25]:

$$b < z < h;\ \frac{\partial C_i}{\partial t} + \frac{\partial C_i}{\partial x} v_x(z) = D_i \left(\frac{\partial^2 C_i}{\partial x^2} + \frac{\partial^2 C_i}{\partial z^2} \right) \tag{7}$$

where D_i is the molecular diffusion coefficient in the liquid phase and $v_x(z)$ the fluid velocity,

$$v_x(z) = 6U \left[\left(\frac{h-z}{h-b} \right) - \left(\frac{h-z}{h-b} \right)^2 \right] \tag{8}$$

In Eq. (8), U is the cross-section averaged velocity, which is related to the volumetric flow rate Q_v as $U = Q_v/(wh)$. This flow is in steady state, and it involves the no-slip condition at $z = h$ and $z = b$. The connection between Eqs. (2) and (7) is established by the mass flux through the interface,

$$z = b;\ D_i \left(\frac{\partial C_i}{\partial z} \right)_{liquid} = D_{eff} \left(\frac{\partial C_i}{\partial z} \right)_{\text{porous layer}} \tag{9}$$

which is also required to numerically solve the coupled problem. Other boundary condition for Eq. (7) is

$$z = h;\ \frac{\partial C_i}{\partial z} = 0.$$

For the purposes of our analysis below, Eq. (9) is rewritten in terms of the mass transport coefficient k_l as,

$$z = b;\ k_l \left(C_i^0 - C_i^b \right) = D_{eff} \frac{\partial C_i}{\partial z} \tag{10}$$

where C_i° and C_i^b stand for the concentration in feed solution and the interface ($z = b$), respectively. The mass transport coefficient k_l is given by Hansen et al. [18] and Bird et al. [25]:

$$k_l = 1.2819 Pe^{1/3} \frac{D_i}{L^{1/3} h^{2/3}} \tag{11}$$

where $Pe = Uh/D_i$ is the Péclet number, being L the cell length.

In order to simplify the study of the different variables that affect the operative performance of ATR cell, a dimensionless analysis can be carried out. Thus, the mass balance for i-species in the porous layer results,

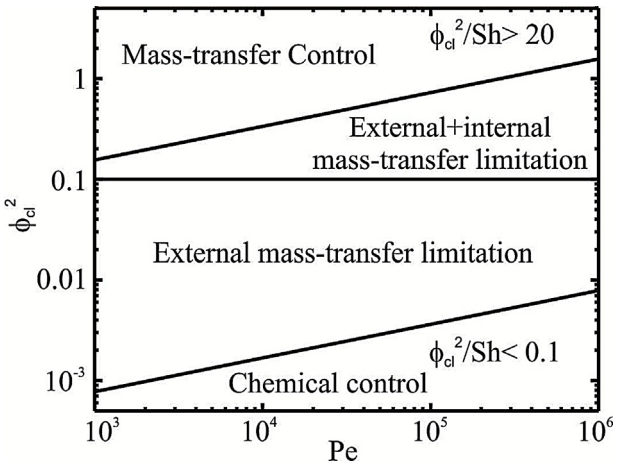

Fig. 3. Operative limits for the ATR cell defined in a Thiele modulus-Péclet number diagram, by using the ϕ_{cl}^2/Sh ratio as criteria to differentiate mass transport regimes.

$$0 < b^* < 1;\ \frac{\partial C_i^*}{\partial \tau_D} = \frac{\partial^2 C_i^*}{\partial b^{*2}} + \frac{\partial^2 C_i^*}{\partial \eta^2} \gamma^2 - \phi_{cl}^2 \left[C_i^* \left(1 - \theta \right) - \overline{K_D} \theta \right] \tag{12}$$

with the following definitions: $C_i^* = C_i/C_i^0, \theta = \Gamma/\Gamma_0$, $\tau_D = \frac{D_{eff}}{b^2} t$, $b^* = z/b, \eta = x/L, \gamma = b/L$, and $\overline{K_D} = \frac{k_d}{k_a C_i^0}$. In particular, ϕ_{cl} is the Thiele modulus for the catalyst layer, as defined in Refs. [21,24]: $\phi_{cl}^2 = \frac{\varepsilon^{-1} a_v k_a \Gamma_0 b^2}{D_{eff}}$. This modulus represents the ratio between the adsorption rate and the diffusivity of the reactant. When $\phi_{cl} \ll 1$, the transport is limited by the reaction, while for $\phi_{cl} \gg 1$ the transport becomes diffusion-limited.

However, this dimensionless number does not take into account the transport by convection. For a more exhaustive analysis, some simplifications of Eq. (12) could be done. Given that b is much smaller than L, one can: (i) remove the diffusive transport in the x-direction from Eq. (12) $b^* = 0$; $\frac{dC_i^*}{db^*} = 0$, and (ii) assume a quasi-steady state $b^* = 1; Sh \left(1 - C_i^{*b} \right) = \frac{\partial C_i^*}{\partial b^*}$ [24]. Then the simplified mass balance is:

$$\frac{d^2 C_i^*}{db^{*2}} = \phi_{cl}^2 C_i^* \tag{13}$$

The respective boundary conditions take the form:

$$b^* = 0;\ \frac{dC_i^*}{db^*} = 0 \tag{14}$$

$$b^* = 1; Sh \left(1 - C_i^{*b} \right) = \frac{\partial C_i^*}{\partial b^*} \tag{15}$$

where, C_i^{*b} is the normalized concentration at the interface and $Sh = k_l b/D_{eff}$ is the Sherwood number [24,25]. This number represents the ratio between the mass transport rate and the diffusion in the catalyst layer.

Eq. (13) can be analytically solved with boundary conditions 14 and 15 to give

$$C_i^* = \frac{\cosh(\phi_{cl}.b^*)}{\cosh(\phi_{cl})} \frac{1}{\Phi} \tag{16}$$

Please cite this article in press as: A. Aguirre, et al., ATR-FTIR spectrokinetic analysis of the CO adsorption and oxidation at water/platinum interface, Catal. Today (2016), http://dx.doi.org/10.1016/j.cattod.2016.03.042

Table 1
Parameters employed for the simulations and corresponding dimensionless numbers.

Simulation	1	2	3
$k_a[M^{-1}s^{-1}]$	3×10^{1}	3×10^{2}	3×10^{3}
ϕ_{cl}^2	3.9×10^{-3}	3.9×10^{-2}	3.9×10^{-1}
ϕ_{cl}^2/Sh	0.088	0.88	8.8

Table 2
Parameters obtained from the fitting of the data presented in Fig. 5 for the oxidation of pre-adsorbed CO on platinum.

Catalyst	f	k_1	k_2	k_3	k_4
Pt/ZnSe	0.385	0.029	0.102	0.064	0.0136
Pt/Al_2O_3	0.469	0.013	0.104	0.144	0.0113

For more details see Supplementary information.

where $\Phi = \left[\frac{\phi_{cl}\cdot\tanh(\phi_{cl})}{Sh}+1\right]$. We have established in Eq. (12) that a necessary condition to avoid gradients in the porous bed is $\phi_{cl}\to 0$. In this limiting case, the Φ parameter is:

$$\Phi = \frac{\phi_{cl}^2}{Sh}+1 \tag{17}$$

Considering the usual propagation of errors involved in the experimental measurement in ATR, the concentration of the reactive species in the surface of the porous bed ($z=b$) must be, at least, 90% of the bulk liquid phase concentration, so that the system is under kinetic control [16]. Hereby, the relation ϕ_{cl}^2/Sh must be less than 0.1. This criterion makes possible to identify the range of operative conditions that can be applied to measure kinetic parameters in our ATR cell.

3. Results and discussion

3.1. Assessment of the operative limits for a porous layer of catalyst

As was described above, a diffusion-convection regime governs the transport of the reactants from the flowing solution to the catalyst layer. Therefore, it is useful to illustrate how the operational limits of the ATR cell can be determined in order to work under chemical control. As an example, the transport model with adsorption was solved numerically with parameters taken from the literature [16]: $D_i = 1\times10^{-6}$ cm^2/s, $D_{eff} = 4\times10^{-7}$ cm^2/s, $\Gamma^\circ = 5\times10^{-12}$ mol/cm^2, $C_i^\circ = 1\times10^{-4}$ M, $Keq = 1\times10^{5}$ M^{-1}, $b = 1$ μm, U+03B5 = 0.5, $a_v = 1.5\times10^{6}$ cm^{-1}. The volumetric flow was $Q_v = 2.2$ mL/min, leading to $Pe\approx10^5$ and Sherwood number, $Sh = 4.4\times10^{-2}$. Table 1 summarizes the parameters values used in the calculations.

Fig. 2 shows the bulk concentration of the reactant as a function of the cell height for different ϕ_{cl}^2/Sh ratios and different positions along the x-direction (near the entrance and near the exit of the ATR cell). The concentration profiles are taken at $t = 12.5$ s, that is, when the concentration in the bulk and the concentration near the IRE reach a steady state in a blank experiment without adsorption, as shown previously [16]. As seen in Fig. 2, the concentration gradient in the z-direction increases with the ϕ_{cl}^2/Sh ratio. For $\phi_{cl}^2/Sh = 0.088$, only a slight concentration gradient is observed, which enable measurements under the kinetic control, in agreement with the pre-fixed criteria.

To summarize, the operative limits of the ATR cell for the case of adsorption on a catalyst layer are given in Fig. 3, by using the Thiele modulus as a function of the Péclet number. The lower line corresponds to $\phi_{cl}^2/Sh < 0.1$, as required to fulfill the chemical control regime, e.g. 90% of actual rate. At higher ϕ_{cl}^2/Sh ratio, an intermediate regime is found where the observed reaction rate is influence by both intrinsic kinetics as well as external mass-transfer. In this zone, kinetic parameters could be also obtained by solving numerically the full model (convection-diffusion and adsorption/reaction rates). Then, for $\phi_{cl}^2 > 0.1$ mass-transfer limitations by diffusion inside the catalyst layer (internal mass-transfer resistance) are present.

Finally, the highest region of the plot represent the condition of severe mass-transport control (diffusive control), where intrinsic kinetic values cannot be obtained. This graphic chart serves as a practical guide to determine the operational limits of an ATR cell with a porous layer of catalyst deposited onto the IRE.

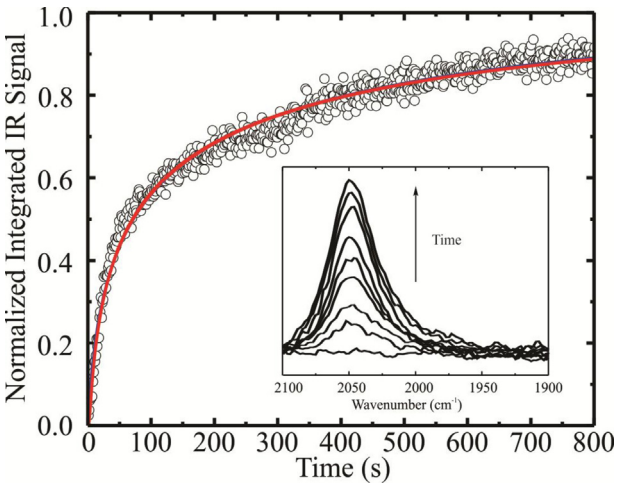

Fig. 4. Evolution of the normalized IR signal of Pt–CO (2048 cm^{-1}) during the adsorption of CO on Pt/Al_2O_3 layer (open circles). Full lines are the best fitting of the data considering the complete convection–diffusion model (red line) and only Eq. (18) (blue line). For the complete model the results are: $k_a^\circ = 34\pm3$ M^{-1} s^{-1} and $\alpha = 8.9\pm2.5$ kJ/mol. Solving the differential equation are: $k_a^\circ = 30\pm3$ M^{-1} s^{-1} and $\alpha = 8.5\pm2.4$ kJ/mol. (For interpretation of the references to color in this figure legend, the reader is referred to the web version of this article.)

3.2. CO adsorption on Pt/Al_2O_3 thin film

The adsorption of CO dissolved in water on a Pt(0.38%)/γ-Al_2O_3 catalyst deposited on a ZnSe IRE is studied. Time-resolved IR spectra were acquired during the CO/H_2O flow into the cell (Fig. 4). Infrared peak at 2048 cm^{-1}, assigned to linear or on-top Pt–CO [3,5], increased its intensity until saturation was reached. A slight shift of ca. 5 cm^{-1} was observed do to the increasing CO coverage [5]. Additionally, a very low band at 1810 cm^{-1} due to bridged CO was detected, but the following analysis is focused on the linear Pt–CO.

The normalized integrated absorbance, representing the fractional coverage of Pt–CO, as a function of time is presented in Fig. 4 ($Q_v = 2.0$ mL/min, $Pe = 5.2\times10^3$). The CO concentration was 9.3×10^{-4} mol/L and the diffusion coefficient of CO in water was $D_i = 1.93\times10^{-5}$ cm^2/s (calculated with the Stokes–Einstein equation [25]). Also for the Pt/Al_2O_3 catalyst layer, $a_v\Gamma_0 = 1.58\times10^{-5}$ mol/cm^3, $\varepsilon = 0.6$ and the effective diffusion coefficient $D_{eff} = 0.4D_i$ [26] (For more details see SI).

The shape of the registered curve cannot be fitted using Eq. (1). The shape of the adsorption curve is similar to the one reported for the CO adsorption on platinum thin films and platinum dispersed on alumina monitored by in situ ATR [5,27–29]. The Tempkin isotherm, that is a linear variation of the heat of adsorption (E) with the coverage, is used to represent the adsorption of CO on platinum. For instance, Bianchi and coworkers reported a $E(\theta=0) = 200$ kJ/mol and $E(\theta=1) = 115$ kJ/mol in supported platinum catalysts by means of variable temperature infrared spectroscopy to measure the isobaric heats of adsorption

Please cite this article in press as: A. Aguirre, et al., ATR-FTIR spectrokinetic analysis of the CO adsorption and oxidation at water/platinum interface, Catal. Today (2016), http://dx.doi.org/10.1016/j.cattod.2016.03.042

Table 3
Calculated dimensionless numbers used to assess the occurrence of the transport limitations during the oxidation of pre-adsorbed CO.

Catalyst	$r_{ads}^{max}(s^{-1})$	*Bi*	*Da*	ϕ_{cl}^2	ϕ_{cl}^2/Sh
Pt/ZnSe	0.0142	0.13	0.025	–	–
Pt/Al_2O_3	0.0183	–	–	6.21×10^{-4}	0.01

r_{ads}^{max}: is the highest rate of adsorption of oxygen on platinum (see text for details).

[30]. Likewise, the sticking çoefficient, or in other words the rate of adsorption, also has been reported to be linearly dependent of the coverage [31]. Then, in this case, the evolution of the surface concentration for the irreversible adsorption of CO takes the form:

$$\frac{d\Gamma_{CO}}{dt} = \left[k_a^0 \exp(-\frac{\alpha \frac{\Gamma_{CO}}{\Gamma_0}}{RT})\right] C_{CO}^0 (\Gamma_0 - \Gamma_{CO}) \quad (18)$$

where the term between brackets stands for the variation of the k_a with the coverage; k_a° is the adsorption rate at coverage zero; C_{CO}° is the concentration of dissolve CO, Γ_0 is the total number of sites, Γ_{CO} is the surface coverage of CO and α is the sticking factor.

The adsorption of CO on platinum at 298 K is irreversible. After saturation, the cell was purged with pure water and the signal of Pt–CO remains stable for more than 1 h. This result confirms the high stability of the adsorbed CO on platinum at room temperature and justify that the desorption rate can be considered as zero ($k_d = 0$).

Note here that the above adsorption model is equal to Eq. (1) at low coverage, were k_a is a maximum. With the aim to estimate the influence of mass transport in the kinetic process using the criteria described in Section 3.1, the k_a at initial coverage was calculated, that is, the more demanding condition. The value obtained by fitting the experimental data was k_a (t = 0) = 29 M^{-1} s^{-1}. Then, $\phi_{cl}^2 = 2.6 \times 10^{-3}$ and $\phi_{cl}^2/Sh = 0.032$. These results show that under this experimental condition the criteria for chemical control are fulfilled (see Fig. 3). Fig. 4 shows the fitting of the experimental data by using both the differential Eq. (18) only, and the complete diffusion-convection model coupled to Eq. (18). As can be seen from the figure, the fitting of the data is satisfactory with both models, confirming that adsorption process is under chemical control.

3.3. Oxidation of pre-adsorbed carbon monoxide in aqueous phase

The oxidation of pre-adsorbed CO in aqueous phase was studied in the Pt/Al_2O_3 catalyst layer, and, also, in a non-porous thin film of platinum deposited into the ZnSe crystal. In a previous work [16], we studied the adsorption of CO on the Pt/ZnSe system. It was shown that, using similar conditions than here, the CO adsorption process is under chemical control.

After adsorption of CO on Pt/ZnSe and Pt/Al_2O_3, the cell was purged with pure water for 1 h in order to eliminate the CO from the liquid phase. The signal from Pt-CO_L (2053 cm^{-1}) remained constant during this time, indicating that CO did not desorb at room temperature. Next, the flow was changed from pure water to O_2/H_2O in order to investigate the oxidation of pre-adsorbed CO on Pt/ZnSe and Pt/Al_2O_3. Fig. 5a and 5b shows the evolution of normalized integrated peak area of linearly adsorbed CO during oxidation. Both systems presented a very similar feature for the change in the CO coverage, with fast decrease during the first ca. 150 s and a low decrease after that time. Similar results were reported for the aqueous oxidation of CO on Pt/Al_2O_3 [27,29,32]. It should be noticed that IR spectra of CO adsorbed on Pt/ZnSe have a much higher signal-to-noise ratio than the spectra collected on Pt/Al_2O_3 system. This can be ascribed to the well-known surface enhanced IR absorption

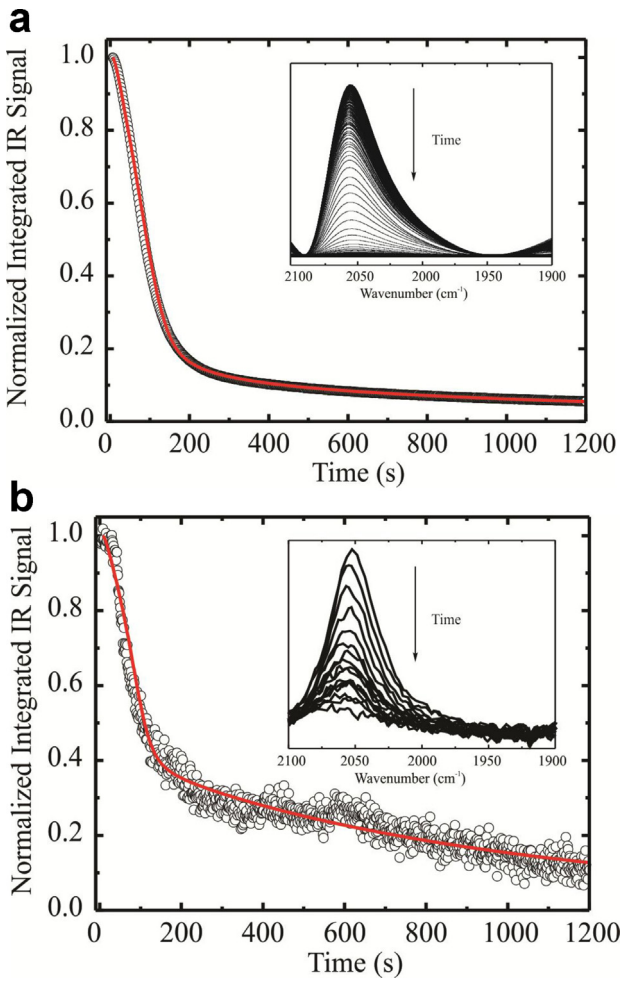

Fig. 5. Evolution of the normalized IR signal of Pt-CO (2048 cm^{-1}) as function of time for oxidation of pre-adsorbed carbon monoxide on (a) Pt/ZnSe and (b) Pt/Al_2O_3. Full line represents the best fitting of the relative surface coverage of CO on each sites: $\bar{A} = \theta_{CO}^{I}(1-f) + \theta_{CO}^{II} f$ (see text for details) considering the microkinetic model for CO oxidation.

(SEIRA) usually found after adsorption of molecules on metal films [1].

The decay of the CO coverage during the oxidation could not be fitted with a simple -one site- Langmuir-Hinshelwood mechanism as show in Fig. S1 (see Supplementary information). CO oxidation on Pt was extensively studied in the literature of surface science (ultra-high vacuum) and electrochemistry processes (liquid phase) [33–45]. From the work of Ertl and co-workers [35], it is generally accepted that CO adsorbed on Pt low-coordination sites is oxidized by adsorbed oxygen atoms (Langmuir–Hinshelwood mechanism). In turn, CO on high-coordination Pt sites is not directly oxidized, but only after surface diffusion to low-coordination sites [39]. Then, the following reaction steps for the CO oxidation have been proposed:

(i) CO adsorption on low or high-coordination Pt sites:

$$CO + Pt_{IorII} \rightarrow CO - Pt$$

(ii) Dissociative adsorption of O_2 on low-coordination Pt sites [39]:

$$O_2 + 2Pt_I \rightarrow 2O - Pt_I$$

(iii) CO oxidation on low-coordination Pt sites:

$$CO - Pt_I + O - Pt_I \rightarrow CO_2 + 2Pt_I$$

Please cite this article in press as: A. Aguirre, et al., ATR-FTIR spectrokinetic analysis of the CO adsorption and oxidation at water/platinum interface, Catal. Today (2016), http://dx.doi.org/10.1016/j.cattod.2016.03.042

(iv) Interconversion of CO from high-coordination sites (Pt_{II}) to low-coordination sites (Pt_I):

$$CO - Pt_{II} + Pt_I \rightarrow CO - Pt_I + Pt_{II}$$

The corresponding differential equations to describe the mechanism are:

$$\frac{d\theta^I_{CO}}{dt} = k_a C_{CO}(1 - \theta^I_{CO} - \theta^I_O) + fk_1\theta^{II}_{CO}\left(1 - \theta^I_{CO} - \theta^I_O\right) - k_2\theta^I_{CO}\theta^I_O \quad (19)$$

$$\frac{d\theta^{II}_{CO}}{dt} = k_a C_{CO}(1 - \theta^{II}_{CO}) - (1-f)k_1\theta^{II}_{CO}\left(1 - \theta^I_{CO} - \theta^I_O\right) \quad (20)$$

$$\frac{d\theta^I_O}{dt} = k_3 C^*_{O_2}\left(1 - \theta^I_{CO} - \theta^I_O\right)^2 + k_4 C^*_{O_2}\left(1 - \theta^I_O\right)^2 - k_2\theta^I_{CO}\theta^I_O \quad (21)$$

where, f stand for the ratio of low- to high-coordination sites ($f = \Gamma^{II}_{Pt}/\Gamma^0_{Pt}$), θ^I_{CO} and θ^{II}_{CO} are the relative surface coverage of CO on each sites, θ^I_O is the relative surface coverage of oxygen on low-coordination sites; k_i stand for the apparent kinetic constant for each step (described in detail in Supplementary information), and $C^*_{O_2}$ is the normalized oxygen concentration at the interface.

This set of differential equations was numerically integrated (fourth order Runge–Kutta) and the error between the model and the experimental data was minimized with f and the k_i as fitting parameters (Down-Simplex). The error between the model and the experimental data was calculated by setting as the normalized integrated IR signal ($\bar{A}$) the sum of the relative surface coverage of CO on each sites: $\bar{A} = \theta^I_{CO}(1-f) + \theta^{II}_{CO}f$. Full lines in Fig. 5a and brepresent the best fits to experimental data. As seen in the figure, this model satisfactorily represents the obtained results. The calculated parameters are listed in Table 2.

With the aim to estimate the influence of mass transport in the kinetic process, an analysis was performed based on the criteria described in Section 3.1. In the studied case, the mass transport limitation come from the diffusion of dissolved oxygen from the solution to the liquid/solid interface. Then, the highest gradient in oxygen concentration ($C^{bulk}_{O_2} - C^{interphase}_{O_2}$) occurs when the consumption of oxygen at the interface is maximum, in other words, when the rate of adsorption and oxidation reach a maximum (r^{max}_{ads}). Therefore, we estimate the *Bi* and *Da* numbers for the Pt/ZnSe [16] and the *Sh* and ϕ^2_{cl} numbers for Pt/Al_2O_3 at that condition, which is a conservative position in order to assess the presence of mass transport limitations. According to the model, see Supplementary information, this condition occurs at 92 s for the Pt/Al_2O_3 and at 97 s for Pt/ZnSe. Table 3 presents the results for the calculated dimensionless numbers for each case. For the CO oxidation on Pt/ZnSe, the calculated value of the *Da* number is 0.025. This values fulfill the criteria stablished for a process under chemical control in a non-porous film, e.g. $Da < 0.1$ [16].

For the porous Pt/Al_2O_3 system, the analysis is more complex. As discussed in Section 3.1 the mass transference limitation could occur: (i) external to the porous layer, (ii) into the catalyst layer, and (iii) into the catalyst particles. We showed before that the criteria developed based on the ϕ^2_{cl} and the *Sh* numbers can be used to stablish the presence of mass transfer limitations. The calculated values for this system are $\phi^2_{cl} = 6.2 \times 10^{-4}$ and $\phi^2_{cl}/Sh = 0.01$ ($Pe = 4 \times 10^3$ for oxygen in water). These values lay below the limit displayed in Fig. 3 for the condition of chemical control, confirming that the CO oxidation processes in under chemical control during the measurement.

4. Conclusions

The mass-transfer limitations for in situ and operando spectrokinetic investigations in an optimized flow-through ATR cell were investigated. For a layer of porous catalyst deposited into the ATR crystal, the transport from the liquid phase to the layer and the internal mass transport were modeled and the operational limits were characterized in terms of Péclet (*Pe*) and Sherwood (*Sh*) numbers, and Thiele modulus (φ_{cl}). In order to obtain kinetic data under true chemical control, suitable criteria were presented considering the geometry and experimental flow rates. Results show that, for the porous film case, the internal mass transport (i.e. the diffusion in the porous layer) could be neglected for low φ_{cl}; and the external mass transport (i.e. the transport from the liquid phase to the film) is not present for values of $\phi^2_{cl}/Sh < 0.1$. This condition allows determining elemental kinetic constants under chemical control and it is expected that help to the development of quantitative models for spectroscopic cells and improves the capabilities of operando methodology.

The adsorption and oxidation of CO was studied on a layer of $Pt(0.38\%)/Al_2O_3$ and on a Pt thin film deposited on a ZnSe. The evolution of the infrared signal of Pt-CO surface species was fitted with an adsorption and oxidation microkinetic models. To the best of our knowledge this is the first kinetic model of CO oxidation in liquid phase. The kinetic constants experimentally obtained fulfill the criteria developed to determine the presence of transport limitations, showing that the investigated processes are under chemical control.

Acknowledgments

Financial support from the Consejo Nacional de Investigaciones Científicas y Técnicas (CONICET), PIP-2014-11220130100086CO, Universidad Nacional del Litoral (UNL) CAID-0100; and Agencia Nacional para la Promoción de la Ciencia y Tecnología of Argentina (ANPCyT) PICT-2014-0497 is gratefully acknowledged. A.A. thanks CONICET for the fellowship received to carry out this work.

Appendix A. Supplementary data

Supplementary data associated with this article can be found, in the online version, at http://dx.doi.org/10.1016/j.cattod.2016.03.042.

References

[1] T. Bürgi, A. Baiker, Adv. Catal. 50 (2006) 227–283.
[2] H. Shi, J.A. Lercher, X.Y. Yu, Catal. Sci. Tech. 5 (2015) 3035–3060.
[3] B.L. Mojet, S.D. Ebbesen, L. Lefferts, Chem. Soc. Rev. 39 (2010) 4643–4655.
[4] I. Dolamic, T. Bürgi, J. Phys. Chem. C 115 (2011) 2228–2234.
[5] D. Ferri, T. Bürgi, A. Baiker, J. Phys. Chem. B 105 (2001) 3187–3195.
[6] V. Choudhary, S.H. Mushrif, C. Ho, A. Anderko, V. Nikolakis, N.S. Marinkovic, A.I. Frenkel, S.I. Sandler, D.G. Vlachos, J. Am. Chem. Soc. 153 (2013) 3997–4006.
[7] A. Maclennan, A. Banerjee, Y.F. Hu, J.T. Miller, R.W.J. Scott, ACS Catal. 3 (2013) 1411–1419.
[8] M. Nielsen, E. Alberico, W. Baumann, H.J. Drexler, H. Junge, S. Gladiali, M. Beller, Nature 495 (2013) 85–90.
[9] J.M. Andanson, A. Baiker, Chem. Soc. Rev. 39 (2010) 4571–4584.
[10] A.G. Young, A.J. McQuillan, Langmuir 25 (2009) 3538–3548.
[11] A. Aguirre, A. Bonivardi, S. Matkovic, L. Briand, S.E. Collins, Top. Catal. 54 (2011) 229–235.
[12] A. Urakawa, R. Wirz, T. Bürgi, A. Baiker, J. Phys. Chem. B. 107 (2003) 13061–13068.
[13] M. Bieri, T. Bürgui, J. Phys. Chem. B 109 (2005) 10243–10250.
[14] F. Meemken, P. Müller, K. Hungerbühler, A. Baiker, Rev. Sci. Instrum. 85 (2014) 084101–084117.
[15] F.C. Meunier, Chem. Soc. Rev. 39 (2010) 4602–4614.
[16] A. Aguirre, P.A. Kler, C.L.A. Berli, S.E. Collins, Chem. Eng. J. 243 (2014) 197–206.
[17] T. Gervais, K. Jensen, Chem. Eng. Sci. 61 (2006) 1102–1121.
[18] R. Hansen, H. Bruus, T.H. Callisen, O. Hassager, Langmuir 28 (2012) 7557–7563.
[19] K.F. Jensen, Chem. Eng. Sci. 56 (2001) 293–303.
[20] J.P. Lopes, S.S. Cardoso, A.E. Rodrigues, Chem. Eng. J. 116-177 (2011) 3–13.
[21] J.P. Lopes, S.S. Cardoso, A.E. Rodrigues, Chem. Eng. J. 227 (2013) 42–55.
[22] St. Walter, St. Malmberg, B. Schmidt, M.A. Liauw, Catal. Today 110 (2005) 15–25.
[23] L. Kiwi-Minsker, A. Renken, Catal. Today 110 (2005) 2–14.

[24] G.F. Froment, K.B. Bischoff, J. DeWilde, Chemical Reactor Analysis and Design, third ed., J. Wiley, New York, 2011.
[25] R. Bird, W.E. Stewart, E.N. Lightfoot, Transport Phenomena, second ed., J. Wiley, New York, 2002.
[26] R.H. Perry, D.W. Green, Perry's Chemical Engineers' Handbook, seventh edition, McGraw-Hills, New York, 1999.
[27] S.D. Ebbesen, B.L. Mojer, L. Lefferts, Langmuir 22 (2006) 1079–1085.
[28] S.D. Ebbesen, B.L. Mojet, L. Lefferts, J. Catal. 246 (2007) 66–73.
[29] I. Ortiz-Hernandez, C.T. Williams, Langmuir 19 (2003) 2956–2962.
[30] A. Bourane, O. Dulaurent, K. Chandes, D. Bianchi, Appl. Catal. A. 214 (2001) 193–202.
[31] A.W. Adamson, Physical Chemistry of Surfaces, fifth edition, J. Wiley & Sons Inc., New York, 1990.
[32] B.L. Mojet, S.D. Ebbesen, L. Lefferts, Chem. Soc. Rev. 39 (2010) 4643–4655.
[33] M.A. Barteau, E.I. Ko, R.J. Mmadix, Surf. Sci. 104 (1981) 161–180.
[34] T. Engel, G. Ertl, Advan. Catal. 28 (1979) 1.
[35] R. Imbihl, M.P. Cox, G. Ertl, H. Müller, W. Brenig, J. Chem. Phys. 83 (1985) 1578–1587.
[36] R. Imbihl, G. Ertl, Chem. Rev. 95 (1995) 697–773.
[37] G. Ertl, P.R. Norton, J. Rustig Phys. Rev. Lett. 2 (1982) 177–180.
[38] G. Ertl, Adv. Catal. 45 (2000) 1–69.
[39] V.P. Zhdanov, Surf. Sci. Rep. 45 (2002) 231–326.
[40] V.I. Elokhina, A.V. Matveeva, E.V. Kovalyova, V.V. Gorodetskii, Chem. Eng. J. 154 (2009) 94–106.
[41] J. Lauterbach, G. Bonilla, T.D. Pletcher, Chem. Eng. Sci. 54 (1999) 4501–4512.
[42] D. Zhang, O. Deutschmann, Y.E. Seidel, R.J. Behm, J. Phys. Chem. C 115 (2011) 468–478.
[43] C.A. Angelucci, E. Herrero, J.M. Feliu, J. Phys. Chem. C 114 (2010) 14154–14163.
[44] S. Gilman, J. Phys. Chem. 68 (1964) 70–80.
[45] N.P. Lebedeva, A. Rodes, J.M. Feliu, M.T.M. Koper, R.A. van Santen, J. Phys. Chem. B 106 (2002) 9863–9872.

Please cite this article in press as: A. Aguirre, et al., ATR-FTIR spectrokinetic analysis of the CO adsorption and oxidation at water/platinum interface, Catal. Today (2016), http://dx.doi.org/10.1016/j.cattod.2016.03.042